Polyhedron 261 (2024) 117101

Contents lists available at ScienceDirect

Polyhedron

journal homepage: www.elsevier.com/locate/poly

M(TEIM) complexes with M as Co and Fe: Analogues of classic M(TIM)

Jeremy J. Roos, Prakhar Gautam, Maximilian P. Martin, Leobardo Rodriguez Segura, Andrew T. Poore, Shiliang Tian, Aanuoluwapo E. Adeniyi, Justin L. Andrews, Tong Ren *

Department of Chemistry, Purdue University, West Lafayette, IN 4790, United States

ARTICLE INFO

Keywords:
Cobalt
Iron
Macrocycles
Ligand design

ABSTRACT

The syntheses and characterization of Fe and Co complexes supported by a new tetra-imine macrocycle, TEIM (2,3,9,10-tetraethyl-1,4,8,11-tetraazacyclotetradeca-1,3,8,10-tetraene), are reported. Templating with Co $(OAc)_2{\cdot}4H_2O$ yielded *trans*-$[Co(TEIM)Cl_2][PF_6]$ (**1a**), which was converted to *trans*-$[Co(TEIM)X_2][PF_6]$ (X = N_3 (**2a**) and NO_2 (**3a**)) through reactions with NaX (X = N_3 or NO_2). Templating with Fe generated *trans*-$[Fe(TEIM)(NCCH_3)_2][PF_6]_2$, which was oxidized to *trans*-$[Fe(TEIM)Cl_2][PF_6]$ (**1b**). The reaction of **1b** with NaN_3 formed $[Fe(TEIM)(N_3)_2][PF_6]$ (**2b**) while the reaction with $[Fe(TEIM)(NCCH_3)_2][PF_6]_2$ and $NaNO_2$ yielded *trans*-$[Fe(TEIM)(NO_2)_2]$ (**3b**). Single crystal X-ray diffraction studies revealed a pseudo-octahedral geometry around the Co / Fe centers with the ethyl groups oriented above or below the plane of the TEIM ring. The absorption spectra of **1b** displays weak charge transfer bands near the UV to visible region, while **2b** and **3b** displayed intense charge transfer bands within the visible region. Cyclic voltammograms of **1a** revealed four 1 e^- reductions while those of **2a** and **3a** display only three cathodically shifted reductions. Analogous studies of **1b** and **2b** revealed two 1 e- reductions while **3b** displays only an oxidation event. EPR studies of ferric complexes **1b** and **2b** indicated a low spin d^5 electronic figuration with S = ½ ground state.

1. Introduction

Since the initial report of Co^{III}(TIM) complexes (TIM = 2,3,9,10-tetramethyl-1,4,8,11-tetraazacyclotetradeca-1,3,8,10-tetraene) by Busch and coworkers, [1,2] research efforts of metal complexes of both TIM and related tetra-imine macrocycles have contributed to both the enrichment of basic inorganic chemistry and applications in diverse areas. Electrocatalytic hydrogen evolution by $Co(dmgBF_2)_2(CH_3CN)_2$ ($dmgBF_2$ = difluoroboryl-dimethylglyoxime) and $[Co(TIM)Br_2]^+$ has been studied extensively [3]. Thorough interrogation of Fe(TIM) complexes by Hess and Wieghardt revealed that two of the observed cathodic reductions are in fact localized on the α-diimine units, which led to a postulation of ligand non-innocence through storing two electrons in the form of $(TIM)^{-2}$ and releasing them on demand [4,5]. An unexpected non-innocent behavior of TIM was discovered in the reactions of $[Co^{III}(TIM)Cl_2]^+$ with electron-rich terminal alkynes (HC_2Y): deprotonation of a methyl substituent of TIM enables the formation of 1-aza-2-cobalt-cyclobutene through a [2 + 2] addition of the C≡C bond across a Co-N bond [6,7]. The potential of realizing photo-active M(tetra-imine) complexes is illustrated in the case of $Fe^{II}(HMTI)(CN)_2$ (HMTI = 5,5,7,12,12,14-hexamethyl-1,4,8,11-tetraazacyclotetradeca-1,3,8,10-tetraene), which exhibits an exceptionally long-lived MLCT state ($\tau = 1.25\ ns$) [8].

It has been noted during the course of developing photo-active compounds based on Fe / Co TIM complexes that the low solubility of $[M(TIM)Cl_2][PF_6]$ in organic solvents often presents a challenge towards new syntheses. To circumvent this hurdle, we have attempted and succeeded in the templated synthesis of $[M(TEIM)Cl_2][PF_6]$ (M = Fe, Co), where TEIM (2,3,9,10-tetraethyl-1,4,8,11-tetraazacyclotetradeca-1,3,8,10-tetraene) is the analogue of TIM with the methyl groups replaced by ethyl groups (see Scheme 1). Described herein are the synthesis and characterization of these new complexes and their simple derivatives.

2. Experimental

2.1. Chemicals, reagents, and materials

Literature procedures were followed in the preparation of TMD•2HCl [1]. 3,4-Hexanedione was purchased from Ambeed, and sodium nitrite was purchased from J.T. Baker. $Co(OAc)_2$•$4H_2O$, $FeCl_3$, and sodium azide were purchased from ACROS Organics. Fe powder and

* Corresponding author.
E-mail address: tren@purdue.edu (T. Ren).

https://doi.org/10.1016/j.poly.2024.117101
Received 14 March 2024; Accepted 10 June 2024
Available online 10 June 2024

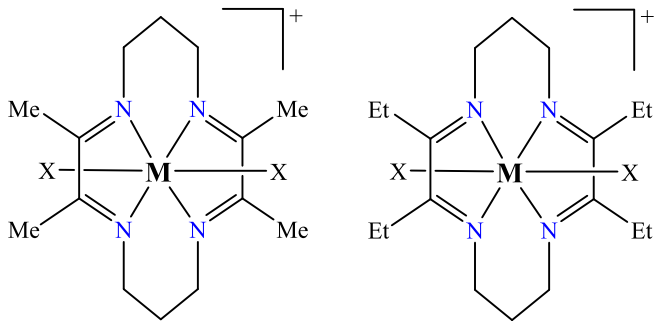

Scheme 1. Metal complexes of classic TIM and new TEIM ligands.

potassium acetate were purchased from Mallinckrodt. $SnCl_2$ was purchased from Oakwood Chemical, and 1,3-diaminopropane was purchased from Sigma-Aldrich. All reagents were used as received. All inert atmosphere manipulations were performed using Schlenk line techniques with nitrogen gas. $[Fe(TEIM)(NCCH_3)_2][PF_6]_2$ was prepared using a modified procedure similar to that reported in literature for $[Fe(TIM)(NCCH_3)_2][PF_6]_2$ (See SI for experimental details) [9].

2.2. Physical measurements

UV–vis-NIR spectra were collected on a JASCO V-780 UV–Vis-NIR spectrophotometer. IR spectra were recorded using a JASCO FT-IR 6700 equipped with a ZnSe crystal ATR accessory. Electron-spray ionization mass spectra were obtained using an Advion Mass Spectrometer. ^1H and ^{13}C NMR spectra were recorded with a Varian INOVA300 NMR (referenced to solvent residuals in CD_3CN or $CDCl_3$). Cyclic voltammograms were recorded for 1 mM solutions in CH_3CN, CH_2Cl_2 or THF (0.1 M tetrabutylammonium hexafluorophosphate) under argon with a glassy carbon working electrode, platinum counter electrode, and Ag/AgCl pseudo-reference electrode (with ferrocene as an external standard). These were recorded on a CHI620A potentiostat. Elemental analyses for the Co complexes were performed by Atlantic Microlab Inc. in Norcross, GA. Elemental analyses for the Fe complexes were obtained in house using an EAI CE440 Elemental Analyser.

2.3. Synthesis of Co(TEIM) complexes

2.3.1. *[Co(TEIM)Cl$_2$][PF$_6$] (**1a**)*

A suspension of TMD•2HCl (5.88 g, 40 mmol) in 100 mL of MeOH was cooled in an ice-water bath prior to the addition of 3,4-hexanedione (4.86 mL, 40 mmol). A methanolic solution (25 mL) of KOH (2.34 g; 41.7 mmol) was added drop-wise to the reaction mixture and stirred for 15 min while capped with a septa to minimize evaporation of the diketone. A suspension of $Co(OAc)_2$•$4H_2O$ (4.98 g, 20 mmol) in 25 mL of MeOH was added slowly to the reaction. Upon stirring for 22 h, 0.5 mL of concentrated HCl was added, and the reaction was stirred for 10 min. A white precipitate was filtered out, and the brown filtrate was collected. Following the addition of KPF_6 (4.6 mg, 25 mmol) dissolved in 30 mL of MeOH, the mixture was stirred for 30 min, during which the crude product precipitated as a light blue-green solid. Following filtration, the product was recrystallized using 100 mL of a 1:1 H_2O/acetone (v/v) mixture with 7 mL of concentrated HCl at 55 °C. Yield: 612 mg (1.17 mmol). The filtrate from the recrystallization was left to evaporate in a filter flask for ~2 weeks, upon which large blue-green crystals formed. These were filtered out, washed thrice with cold MeOH, and dried under vacuum to obtain 188 mg of **1a**. Combined yield: 800 mg (1.53 mmol, 8 % based on Co). ^1H NMR (300 MHz, CD_3CN, ppm): δ = 4.14 – 4.07 (m, 8H), 3.07 (q, 8H, J = 7.7 Hz), 2.50 (qd, 4H, J = 5.8, 2.4 Hz), 1.16 (t, 12H, J = 7.7 Hz); ^{13}C NMR (75 MHz, CD_3CN), ppm): δ = 184.5 (N = *C*C), 52.4 (*N*-*C*C), 27.3 (C*C*C), 25.6 (CC*C*), 10.5 (*C*CH_3); UV/Vis (CH_3CN, nm ($mol^{-1}dm^3cm^{-1}$)):λ_{max} (ε) = 575 (40); 336 (1,100); 262 (17,000); ESI-MS: m/z = 433.13 $[\mathbf{1a}]^+$; elemental analysis calcd (%) for **1a**: C 37.32, H 5.57, N 9.67; found: C 37.23, H 5.59, N 9.58.

2.3.2. *[Co(TEIM)(N$_3$)$_2$ [PF$_6$] (**2a**)*

Compound **1a** (152 mg, 0.26 mmol) was dissolved in 100 mL of a 3/1 MeOH/acetone (v/v) mixture. Upon the addition of NaN_3 (66 mg, 1.02 mmol), the blue-green solution rapidly turned red-brown. The reaction was stirred for 25 min prior to removal of the solvents *in vacuo*. The remaining solid was dissolved in minimal MeCN and recrystallized by the addition of diethyl ether. Compound **2a** was obtained as a microcrystalline brown solid. Yield: 119 mg (0.20 mmol, 77 % based on **1a**). ^1H NMR (300 MHz, CD_3CN, ppm): δ = 3.98–3.89 (m, 8H), 3.04 (m, 8H), 2.29–2.17 (m, 4H), 1.22 (t, 12H, J = 7.7 Hz); ^{13}C NMR (75 MHz, CD_3CN), ppm): δ = 183.6 (N = *C*C), 51.9 (*N*-*C*C), 27.2 (C*C*C), 25.2 (C*C*C), 11.8 (*C*CH_3); IR (cm^{-1}): ν = 2002 (N_3); UV/Vis (CH_3CN, nm ($mol^{-1}dm^3cm^{-1}$)): λ_{max} (ε) = 536 (610); 356 (11,000); ESI-MS: m/z = 447.21 $[\mathbf{2a}]^+$; elemental analysis calcd (%) for **2a**: C 36.49, H 5.44, N 23.64; found: C 36.50, H 5.46, N 23.30.

2.3.3. *[Co(TEIM)(NO$_2$)$_2$][PF$_6$] (**3a**)*

A procedure similar to that of **2a** was performed, except using **1a** (150 mg, 0.26 mmol) and $NaNO_2$ (54 mg, 0.78 mmol). Recrystallization from a yellow MeCN solution and diethyl ether afforded compound **3** as a yellow solid. Yield: 116 mg (0.190 mmol, 75 % based on **1a**). ^1H NMR (300 MHz, CD_3CN, ppm): δ = 4.03–3.93 (m, 8H), 3.08 (q, 8H, J = 7.7 Hz), 2.10–1.98 (m, 4H), 1.25 (t, 12H, J = 7.7 Hz); ^{13}C NMR (75 MHz, CD_3CN), ppm): δ = 186.2 (N = *C*C), 51.4 (*N*-*C*C), 27.7 (C*C*C), 26.0 (C*C*C), 9.9 (*C*CH_3); IR (cm^{-1}):ν = 1420 (NO_2, *asym*), 1301 (NO_2, *sym*); UV/Vis (CH_3CN, nm ($mol^{-1}dm^3cm^{-1}$)): λ_{max} (ε) = 368 (8,100); 259 (11,000). ESI-MS: m/z = 455.18 $[\mathbf{3a}]^+$; elemental analysis calcd (%) for **3a**: C 36.01, H 5.37, N 14.00; found: C 35.78, H 5.39, N 13.74.

2.4. Synthesis of Fe(TEIM) complexes

2.4.1. *[Fe(TEIM)Cl$_2$][PF$_6$] (**1b**)*

An acetone solution of $FeCl_3$ (301 mg, 1.85 mmol) was added dropwise to a solution of $[Fe(TEIM)(NCCH_3)_2][PF_6]_2$ (615 mg, 0.841 mmol) in acetone. The solution was stirred for 1 h, after which the volume was reduced *in vacuo*. The red-brown product was dissolved in minimal CH_2Cl_2 and precipitated with the addition of hexanes. Recrystallization from MeOH/diethyl ether afforded a red-brown solid (**1b**). Yield (**1b**): 440 mg (0.765 mmol, 91 % based on $[Fe(TEIM)(NCCH_3)_2][PF_6]_2$. UV/Vis ($(CH_3)_2CO$, nm ($mol^{-1}dm^3cm^{-1}$)): λ_{max} (ε) = 532 (960); 501 (1,300); 465 (870); 411 (1,700). ESI-MS: m/z = 430.13 $[\mathbf{1b}]^+$; elemental analysis calcd (%) for $FeN_4C_{19}H_{36}P_1F_6OCl_2$ (**1b**•1MeOH): C 37.52, H 5.96, N 9.21; found: C 37.48, H 5.48, N 8.83.

Because of the difficulty in obtaining X-ray quality crystals for $[Fe(TEIM)Cl_2][PF_6]$, the complex ion $[Fe(TEIM)Cl_2]^+$ was crystallized as $[Fe(TEIM)Cl_2][FeCl_4]$, **1b'**. Since the sole purpose of compound **1b'** is X-ray crystallographic analysis, it was not prepared in bulk. Hence, there is no reportable synthetic yield or elemental analysis. Nonetheless, a powder X-ray diffraction pattern collected for compound **1b** (freshly recrystallized from hexanes/acetone, the same solvent combination as for compound **1b'**) was recorded (Fig. S10). The collected pattern clearly differs from the diffractogram of **1b'** (calculated from its CIF, Fig. S10), proving that **1b** and **1b'** are different compounds.

2.4.2. *[Fe(TEIM)(N$_3$)$_2$][PF$_6$] (**2b**)*

Compound **1b** (100.7 mg, 0.175 mmol) was dissolved in MeOH (150 mL) to afford a deep orange solution. NaN_3 (36.8 mg, 0.565 mmol) was added to the methanolic solution and a color change from orange to purple was seen after 1 h. The solution volume was minimized, and diethyl ether was added to precipitate a red solid. Rapid recrystallization from DCM/hexanes provided a bright red powder. Yield: 100.4 mg

(0.171 mmol, 97 % based on **1b**). IR (cm^{-1}): ν = 2002 (N_3); UV/Vis ($(CH_3)_2CO$, nm ($mol^{-1}dm^3cm^{-1}$)): $\lambda_{max}(\varepsilon)$ = 563(6,100); 509(4,100). ESI-MS: *m/z* = 444.22 [**2b**]$^+$; elemental analysis calcd (%) for $FeN_{10}C_{20}H_{36}P_1F_6Cl_4$ (**2b**•2CH_2Cl_2): C 31.64, H 4.77, N 18.45; found: C 31.84, H 4.66, N 18.83.

2.4.3. *[Fe(TEIM)(NO$_2$)$_2$] (3b)*

[Fe(TEIM)(NCCH$_3$)$_2$][PF$_6$]$_2$ (99 mg, 0.136 mmol) was added to 100 mL of MeOH and the red solution stirred for 30 min. $NaNO_2$ (22.9 mg, 0.332 mmol) was added to the solution and stirred for 1 h, resulting in a color change to blue. Solvent volume was reduced *in vacuo* and minimal acetone added to dissolve the blue solid. Hexanes was added to precipitate a blue powder and the resulting product was then eluted over a pad of celite with CH_2Cl_2. Yield: 58 mg (0.128 mmol, 94 % yield based on [Fe(TEIM)(NCCH$_3$)$_2$][PF$_6$]$_2$. ^{1}H NMR (300 MHz, $CDCl_3$, ppm): δ 4.00 (s, 8H), 3.02 (d, 8H, J = 7.9 Hz), 1.96 (s, 4H), 1.31 (t, 12H, J = 7.5 Hz); IR (cm^{-1}): ν = 1536 (NO_2, *asym*), 1331 (NO_2, *sym*); UV/Vis ($(CH_3)_2CO$, nm($mol^{-1}dm^3cm^{-1}$)): $\lambda_{max}(\varepsilon)$ = 658(8,100); 606(5,200). ESI-MS: *m/z* = 452.18 [**3b**]; elemental analysis calcd (%) for $FeN_6C_{20}H_{38}Cl_2$ (**3b**•1CH_2Cl_2, 1MeOH): C 42.19, H 6.73, N 14.76; found: C 42.71, H 6.32, N 14.36.

2.5. X-ray crystallographic analysis

Single crystals of **1a** and **3a** were obtained from the slow diffusion of hexanes into CH_3CN solutions. For the Fe(TEIM) complexes, single crystals of **2b** were obtained through a slow diffusion of hexanes into acetone and of **3b** by slow diffusion of hexanes in CH_2Cl_2. Due to difficulties encountered with the crystallization of complex **1b** using the PF_6^- counterion, single crystals of **1b**' were obtained through a slow diffusion of hexanes in an acetone solution of $FeCl_3$ and **1b**. X-ray diffraction data was obtained on a Bruker Quest diffractometer with Mo-K_α radiation (λ = 0.71073 Å) at 150 K. Data were collected and reflections were indexed and processed using APEX4 [10] and SAINT. The space groups were assigned and the structures were solved by direct methods using XPREP within the SHELXTL suite of programs, [11] and refined using SHELX and SHELXL20 [12–14]. CCDC 2317920–2317924 contain the supplementary crystallographic data for complexes **1a**, **3a**, **1b**', **2b** and **3b**. Powder X-ray diffraction data of **1b** was collected in Bragg-Brentano geometry using a Panalytical Empyrean powder X-ray diffractometer (Cu K-α, λ = 1.54 Å) equipped with a high speed PIXcel 3D Medipix detector. Powder data was collected with sample spinning by continuous scanning within the 2θ range of 5-80° while employing a 1/16° divergence slit, 1/4° anti-scatter slit, and a 4 mm mask.

3. Results and discussion

3.1. Synthesis

As shown in Scheme 2, the Co(TEIM) complexes were prepared through the modification of procedures reported for the Co(TIM) and Co(MePhTIM) analogues [1,15]. The reaction between 3,4-hexanedione and 1,3-diaminopropane dihydrochloride, in the presence of a Co(II) ion, resulted in the templating of the TEIM macrocycle around the cobalt center with axially coordinated chloro ligands. Addition of a methanolic solution of KPF_6 to the crude reaction mixture generated *trans*-[Co(TEIM)Cl$_2$][PF$_6$] (**1a**). Subsequent reactions of **1a** with NaN_3 or $NaNO_2$ yielded *trans*-[Co(TEIM)(N$_3$)$_2$][PF$_6$] (**2a**; 77 %) and *trans*-[Co(TEIM)(NO$_2$)$_2$][PF$_6$] (**3a**; 75 %), respectively, in high yields.

Similarly, the Fe(TEIM) complexes were synthesized through a modification of the reported procedure for the Fe(TIM) complexes [16]. A Schiff base condensation reaction between the 3,4-hexanedione and 1,3-diaminipropane in the presence of acetic acid yielded the TEIM macrocycle. Addition of a methanolic Fe(II) solution to the TEIM macrocycle resulted in the formation of an Fe^{II}(TEIM) species, which was isolated as *trans*-[Fe^{II}(TEIM)(NCCH$_3$)$_2$][PF$_6$]$_2$. *Trans*-[Fe(TEIM)(NCCH$_3$)$_2$][PF$_6$]$_2$ was converted to *trans*-[Fe^{III}(TEIM)Cl$_2$][PF$_6$] (**1b**) through the addition of a saturated acetone solution of $FeCl_3$. Addition of excess NaN_3 to **1b** generated *trans*-[Fe(TEIM)(N$_3$)$_2$][PF$_6$] (**2b**, 97 %). *Trans*-[Fe(TEIM)(NO$_2$)$_2$] (**3b**) was generated, in high yield (94 %), through the addition of excess $NaNO_2$ to a methanolic solution of *trans*-[Fe^{II}(TEIM)(NCCH$_3$)$_2$][PF$_6$]$_2$.

All new Co^{III}(TEIM) complexes are diamagnetic, enabling their characterization via ^{1}H and ^{13}C NMR. Additionally, these complexes were analyzed using ESI-MS, UV–vis-NIR, FT-IR, and elemental analysis. The Fe^{II}(TEIM) complexes are diamagnetic as well, for which ^{1}H NMR were acquired. Both the Fe^{II}(TEIM) and Fe^{III}(TEIM) complexes were further analyzed using ESI-MS, UV–Vis-NIR, FT-IR, and elemental analysis. EPR spectroscopy was used for ascertaining the ground state of the paramagnetic Fe^{III}(TEIM) complexes.

3.2. Solubility analysis

Solubility analyses for **1a** and [Co(TIM)Cl$_2$][PF$_6$] were performed in CH_3OH and acetone following the procedure established by Ouyang and coworkers (see SI for methods) [17]. In contrast to the anticipated improvement in solubility for **1a**, the solubility tests revealed that the [Co(TIM)Cl$_2$]$^+$ complex was more soluble in both acetone and CH_3OH (Table S3). Efforts to determine the solubility in less polar solvents such as THF and CH_2Cl_2 were impeded by the seemingly insolubility of both the Co(TIM) and Co(TEIM) complexes in these solvents.

Similarly, solubility analysis for the **1b** and [Fe(TIM)Cl$_2$][PF$_6$] were performed in CH_3OH, CH_2Cl_2 and acetone (Table S4). The solubility of **1b** was found to be comparable to that of the TIM complex in acetone, and only slightly improved in CH_3OH. However, a significant increase in solubility was observed for **1b** in CH_2Cl_2.

3.3. Molecular structures

Single crystals of **1a** and **3a** were obtained via slow diffusion of diethyl ether into concentrated solutions of CH_3CN. Single crystals of **1b**', **2b**, and **3b** were grown from the slow diffusion of hexanes into solutions of acetone (**1b**' and **2b**) or CH_2Cl_2 (**3b**). The single crystal of **1b**' was obtained with the $FeCl_4^-$ counterion due to the difficulties encountered with crystallization using the PF_6^- counterion. Their molecular structures have been established through single-crystal X-ray

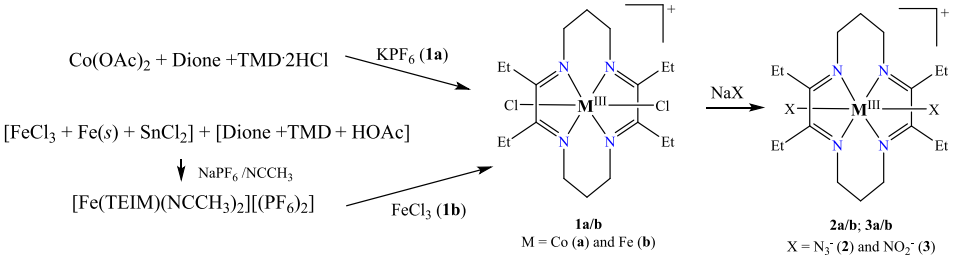

Scheme 2. Syntheses of Co / Fe TEIM complexes. Dione = 3,4-hexanedione; TMD = 1,3- diaminopropane.

diffraction studies. ORTEP plots of the cations are shown in Figs. 1 and 2. The structural studies verify the pseudo-octahedral geometry typical of tetra-imine macrocyclic complexes wherein the macrocycle occupies the equatorial plane, and the remaining ligands occupy the axial sites. All five complexes exhibit a center of inversion at the metal center where two ethyl groups may be oriented above the plane of the macrocycle and the remaining two oriented below the plane. As shown in Scheme 3, the ethyl groups oriented above the plane may exist *cis* (I) or *trans* (II) to each other to impose C_i or C_{2h} symmetry, respectively. Selected bond lengths and angles are provided in Table 1 for the cobalt complexes and Table 2 for the iron species. Details of the data collection can be found in Tables S1 and S2, respectively.

The inner coordination spheres of **1a** and $[Co(TIM)Cl_2]^+$ are highly similar with averaged Co – N bonds lengths of 1.925[1] \AA and 1.926 [1] \AA, respectively [18]. The Co – Cl bond (2.2334(2) \AA) in **1a** is slightly contracted relative to that in Co(TIM) (2.2375[4] \AA); however, this shortening is small and barely above experimental errors (3σ). The lack of significant changes in the equatorial and axial Co ligand bond lengths suggest that the electronic influence of the ethyl groups in the Co(TEIM) complexes is the same as that of the methyl groups in the parent TIM ligand. A similar lack of change to the Co – Cl bond length was observed for *trans*-[Co(2,9-dimethyl-3,10-diphenyl-1,4,8,11-tetraazacyclotetradeca-1,3,8,10-tetraene)Cl_2][PF_6], in which two methyl ligands of the TIM ring were substituted by phenyl rings, as well as for *trans*-[Co(2,3,9,10-tetramethyl-1,4,8,11-tetraazaundeca-1,3,8,10-tetraen-11-ol-1-olate)Cl_2], wherein half of the macrocycle is replaced by an

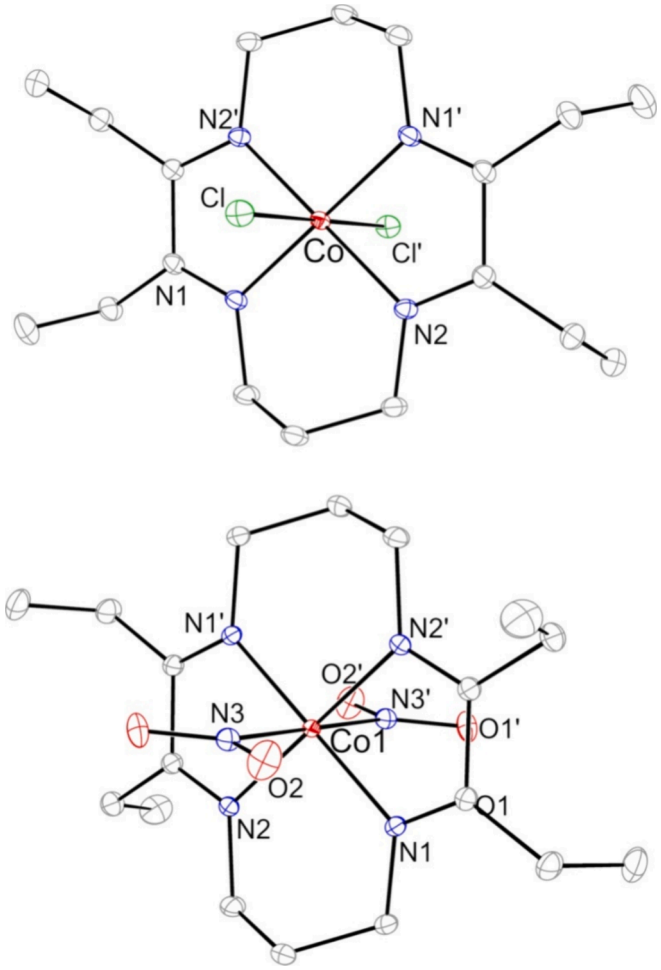

Fig. 1. ORTEP plot of cations $[\mathbf{1a}]^+$ (top) and $[\mathbf{3a}]^+$ (bottom) at 30% probability level; counterions, hydrogen atoms, disorder, and solvent molecules have been omitted for clarity.

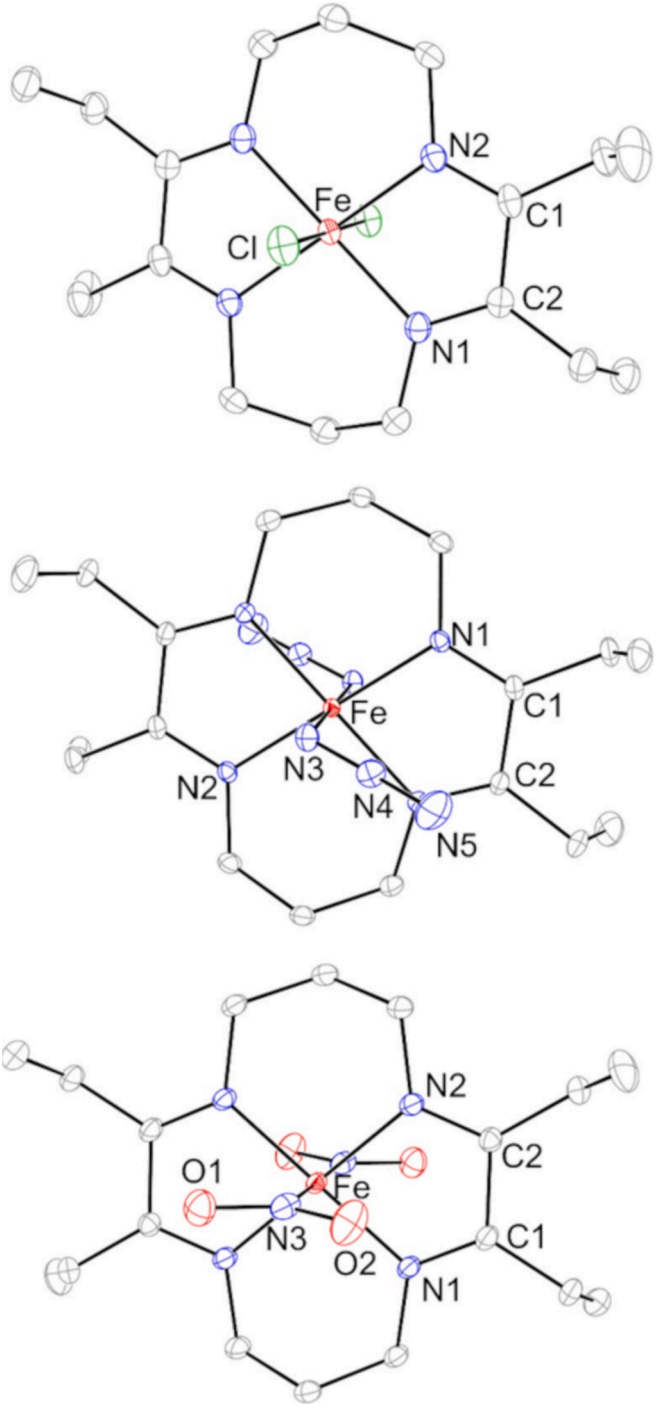

Fig. 2. ORTEP plot of cations $[\mathbf{1b}]^+$ and $[\mathbf{2b}]^+$ and neutral complex [**3b**] at 30 % probability level; counterions, hydrogen atoms, disorder, and solvent molecules have been omitted for clarity.

anionic dioxime moiety [19,20]. The Co – $N_{eq,av}$ bond lengths of **1a** and **3a** (1.919[6] \AA) are also the same, within experimental error. The insensitivity of the equatorial Co – N bonds to the axial ligands is consistent with the postulation that the equatorial ligands and axial ligands are interacting with different sets of Co valence orbitals. The shortened Co – N3 bond length of 1.962[5] \AA in **3a** compared to the Co – Cl in **1a** is attributed to both the smaller atomic radii of nitrogen (0.30 \AA) than chloride (1.67 \AA) and the π-accepting capabilities of the NO_2^- ligands [21]. The latter enables stronger bonding between the cobalt and nitrogen in **3a**, which results in a shorter bond length when

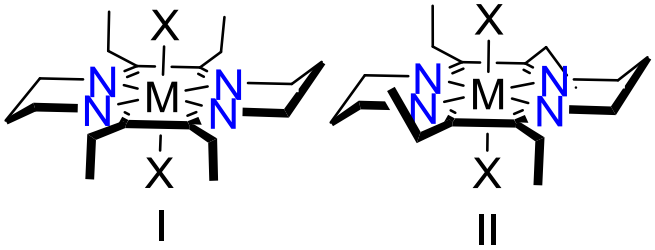

Scheme 3. Possible orientations of the ethyl groups.

Table 1
Selected bond lengths (Å) for $[\mathbf{1a}]^+$, $[\mathbf{3a}]^+$, and $[Co(TIM)Cl_2]^{+\cdot}$.

	$[\mathbf{1a}]^+$	$[\mathbf{3a}]^{+a}$	$[Co(TIM)Cl_2]^{+b}$
$Co–N_{eq,av}$	1.925[1]	1.919[6]	1.926[1]
Co–Cl1/N3	2.2334(2)	1.962[5]	2.2375[4]

[a] Averaged over twelve independent molecules. [b]Ref [18]. [c] Values in brackets indicate averaged s.u. values over multiple moieties.

Table 2
Selected bond lengths (Å) for $[\mathbf{1b}]^+$, $[\mathbf{2b}]^+$, $[\mathbf{3b}]$, and $[Fe(TIM)Cl_2]^{+\cdot}$.

	$[\mathbf{1b}]^+$	$[\mathbf{2b}]^+$	$[\mathbf{3b}]$	$[Fe(TIM)Cl_2]^{+a}$
$Fe–N_{eq,av}$	1.945 [4]	1.945 [1]	1.930 [1]	1.942 [4]
C—C	1.477 (7)	1.4866 (14)	1.4893 (18)	1.475 (5)
N=C	1.290 [9]	1.292 [1]	1.298 [2]	1.290 [5]
Fe–Cl1/N3	2.2429 (12)	1.9620 (8)	1.9807 (10)	2.2518(7)

[a]Ref [22] [b] Values in brackets indicate averaged s.u. values over multiple moieties.

compared to the solely π-donating chloro ligand in **1a**. The Co – N_{ax} are in experimental agreement with those in *trans*-[Co(2,3,9,10-tetramethyl-1,4,8,11-tetraazaundeca-1,3,8,10-tetraen-11-ol-1-olate)$(NO_2)_2$] (1.958[6] \AA), supporting the claim that the equatorial ligands do not affect the axial ligands [20].

There is no significant change in the α-diimine backbone, composed of the N=C and C—C bonds, between the $[Fe(TIM)Cl_2]^+$ and $[Fe(TEIM)Cl_2]^+$ complexes. The Fe – $N_{eq,av}$ bond length for **1b** (1.945[4] Å) is nearly identical to that in $[Fe(TIM)Cl_2]^+$ (1.942[4] Å), indicating that the electronic effects of the ethyl groups on TEIM are identical to the TIM methyl groups. As previously noted above for **1a**, a minor but experimentally significant (>3σ) contraction of the Fe – Cl bond is seen as well for **1b** when compared to the parent Fe(TIM) complex. The Fe – Cl bond for **1b** is consistent with that in an analogous Fe tetraimine complex, *trans*-$[Fe(HMTI)Cl_2]^+$, where the average Fe – Cl bond length is recorded as 2.2476[9] \AA [22]. Additionally, the Fe – $N_{eq,av}$ bond for **1b** matches closely to $[Fe(HMTI)Cl_2]^+$ (1.945[3] \AA), further supporting that the electronic effects of the ethyl groups of TEIM are indistinguishable to the effects of the methyl group on the macrocycle backbone. In comparing **1b** and **2b,** the Fe – $N_{eq,av}$ bond remains unchanged, suggesting that the azido ligands behave as pseudo-halides when coordinated to the Fe^{III} center. Overall, the macrocycle size does not seem to be altered in any substantial manner upon the coordination of the azido ligands.

A comparison of the ferrous **3b** complex to the ferric counterparts **1b** and **2b** reveals no significant change in the bond metrics around the macrocycle. However, the Fe – $N_{eq,av}$ bond (1.930[1] \AA) in **3b** is noticeably shortened despite a larger Fe^{II} ion than the Fe^{III} ion in **1b** and **2b**. The contraction is clearly the result of the coordination of the nitro (NO_2^-) ligand, a π-acceptor, and the loss of Fe electron density to NO_2^- ligands is compensated by stronger σ donation of N_{eq} centers.

3.4. UV–vis spectroscopic analysis

3.4.1. Absorption spectra of Co(TEIM) complexes

The absorption spectra for **1a** – **3a** were collected in acetonitrile and are displayed in Fig. 3. Within the visible region, a *d–d* transition ($^1A_{1g} \rightarrow {}^1T_{1g}$, O_h) can be observed for **1a** and **2a** at 570 nm and 537 nm, respectively. The increased energy for the *d–d* absorption maxima for **2a** is consistent with the stronger field nature of the azido ligands over the chloro ligands in **1a**. Presumably, the *d–d* transition is further blue shifted by the stronger nitro ligands in **3a**; however, it is likely that this band is obscured by the high intensity band at 369 nm. Interestingly, a broad band in **1a** appears within this region between 320 and 415 nm, but it is much weaker, with a molar absorptivity (ε) of ~1,000 $M^{-1}cm^{-1}$. In comparison, the corresponding bands in the nitro- and azido- complexes have molar absorptivity values of 8,100 and 11,000 $M^{-1}cm^{-1}$, respectively. Based on their extinction coefficients, these bands can be assigned as ligand (Cl^-, NO_2^-, and N_3^-)-to-metal charge-transfer bands (LMCT), which is in agreement with previous assignments in $[Co(TIM)X_2]^+$ complexes [18]. Overall, the absorption spectra for **1a** – **3a** are very similar to those of the $[Co(TIM)X_2]^+$, $[Co(MePhTIM)X_2]^+$, and $[Co(MeEtTIM)X_2]^+$analogues [15] indicating that the alkyl substituents on the α-diimine units have the same effect on the electronic properties of the Co^{III} center.

3.4.2. Absorption spectra of Fe(TEIM) complexes

The absorption spectra for **1b** – **3b** recorded in acetone are displayed in Fig. 4, in which the visible region is dominated by charge-transfer bands for all three complexes. For **1b**, the bands centered at *ca.* 502 nm (1,800 $M^{-1}cm^{-1}$) are assigned as LMCT from the chloro lone pairs to the highest occupied Fe *d*-orbitals. For **2b**, an intense charge transfer band is observed at *ca.* 560 nm (6,100 $M^{-1}cm^{-1}$), which is also assigned as an LMCT. Additionally, a noticeable shoulder at 509 nm (4,100 $M^{-1}cm^{-1}$) is observed. The origin of the charge transfers is attributed to an excitation from the π orbitals of the N_3^- ligands to the highest occupied *d*-orbital of Fe. For **3b**, a charge transfer band at *ca.* 659 nm (8,100 $M^{-1}cm^{-1}$) is of similar shape to that of **2b** but the nature of this transition is instead from the fully occupied *d*-orbital of Fe^{II} to the unoccupied π* orbital (MLCT) of the TEIM ligand. A shoulder at 607 nm (5000 $M^{-1}cm^{-1}$) is seen for **3b** as well. All of the above-mentioned assignments are tentative, aided by either the prior study of $Fe(HMTI)(CN)_2$ (for **2b**) [8] or the ground state assignment from the EPR study (for **1b** and **3b**, see the discussion below).

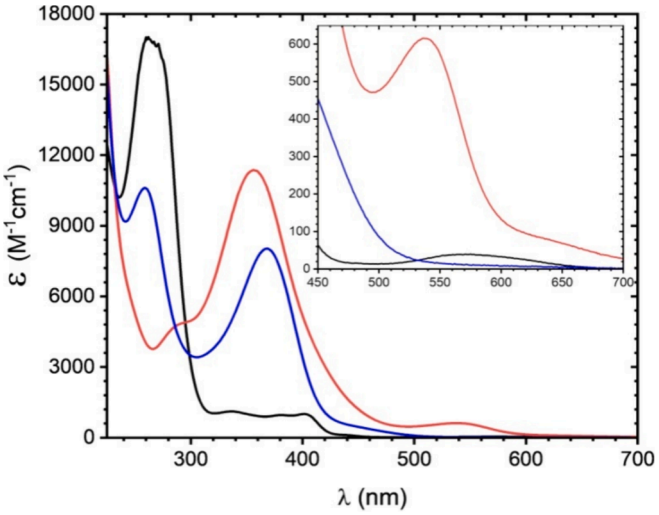

Fig. 3. Absorption spectra of **1a** (black), **2a** (red), and **3a** (blue) in CH_3CN. The inset shows the *d-d* bands. ((Colour online.))

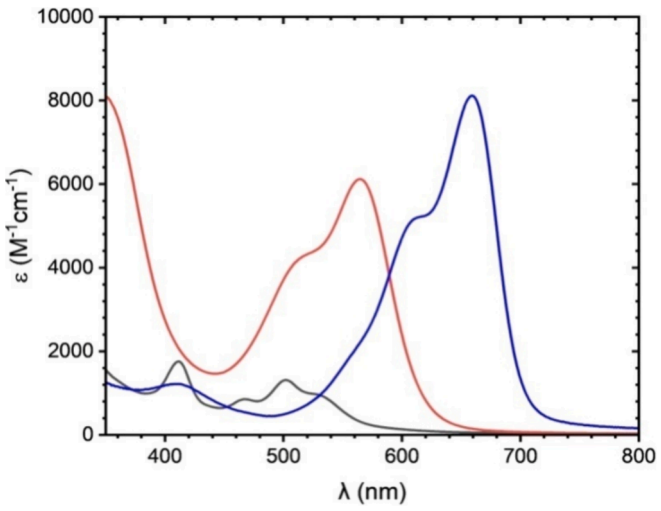

Fig. 4. Absorption spectra of **1b** (black), **2b** (red), and **3b** (blue) in acetone. ((Colour online.))

3.5. Electrochemistry

Voltammetric properties of all complexes were probed and cyclic voltammograms and differential pulse voltammograms are shown in Fig. 5 (**1a**–**3a**) and 6 (**1b**–**3b**) and the redox potentials are reported in Tables 3 (**1a**–**3a**) and 4 (**1b**–**3b**). Due to solubility differences, the voltammograms for **1a**–**1b** were collected in CH_3CN, **1b** and **3b** were collected in CH_2Cl_2, and **2b** was collected in THF.

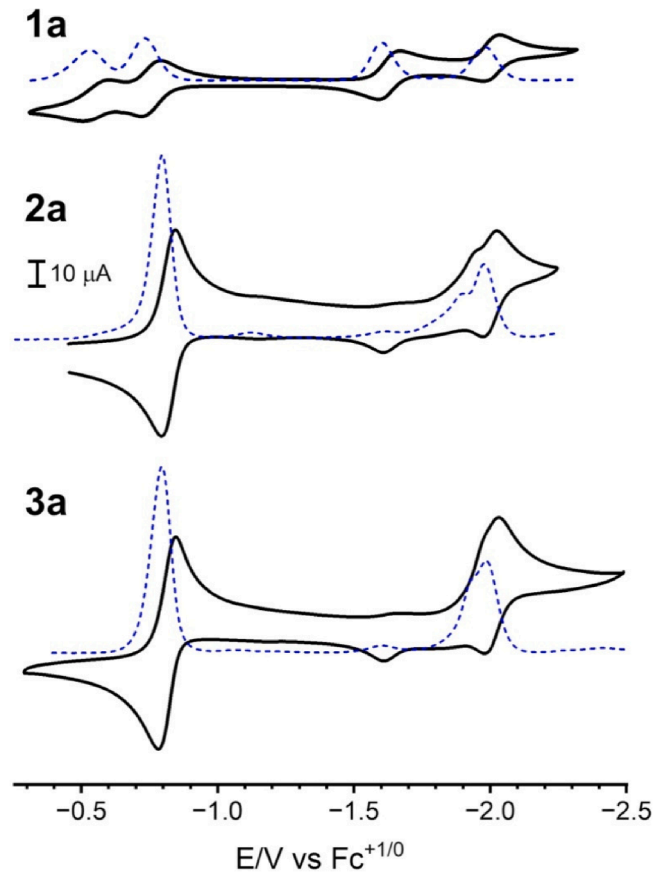

Fig. 5. Cathodic scans of **1a** (top), **2a** (middle), and **3a** (bottom) in 1 mM CH_3CN solutions with 0.1 M *n*-Bu_4NPF_6 as the supporting electrolyte at a 0.1 V/s scan rate.

Table 3
Electrode potentials of observed redox couples (V, vs Fc^+/Fc).

	$E_{pa}(Co^{+4/+3})$	$E_{pc}(Co^{+3/+2})$	$E_{pc}(TEIM^{0/-1})$	$E_{pc}(Co^{+2/+1})$	$E_{1/2}(TEIM^{-1/-2})$
1a	–-	−0.55	−0.75	−1.62	−2.00
2a[a]	1.47	−0.82	––	––	––
3a[a]	–-	−0.81	––	––	––

[a]Reduction events beyond $Co^{+3/+2}$ are not assigned.

3.5.1. Cyclic voltammetry of Co(TEIM) complexes

The cyclic voltammograms for **1a**–**3a** are comparable to their $[Co(TIM)X_2]^+$ counterparts [18]. In the anodic scans, only **2a** exhibits a $1e^-$ irreversible $Co^{+4/+3}$ oxidation event within the CH_3CN solvent window (Fig. S1). This may be attributed to the less electron-withdrawing nature of the azido axial ligands relative to the chloride and nitro ligands of **1a** and **3a**. In the cathodic window, four well-behaved $1e^-$ reductions can be observed. Consistent with the previous assignment for $[Co(TIM)Cl_2]^+$, two reductions are assigned to Co-based reductions and the remaining two are assigned to TEIM-based reductions (see Table 3). For **2a** and **3a**, the reduction pattern is more intricate, and only three events can be observed within the solvent window. Upon the coordination of azido (**2a**) or nitro ligands (**3a**), the $Co^{+3/+2}$ reduction potential is significantly shifted to more negative values of −0.81 V and −0.82 V, respectively. Two additional reduction events can be observed for **2a** and **3a** around −1.96 V and −2.03 V. These peaks are broad and likely the results of the convolution of TEIM-based reductions and the $Co^{+2/+1}$ reduction (Fig. 6. Table 4).

3.5.2. Cyclic voltammetry of Fe(TEIM) complexes

The cyclic voltammetry of **1b** is quite similar to that of $[Fe(TIM)Cl_2]^+$. The cathodic region consists of a reduction at −0.43 V ($Fe^{+3/+2}$) and a subsequent reduction at −0.84 V ($TEIM^{0/-1}$). The $Fe^{+3/+2}$ couple in **1b** is 70 mV more negative than that of $[Fe(TIM)Cl_2]^+$, suggesting that the ethyl substituents are better electron donors to the α-diimines than

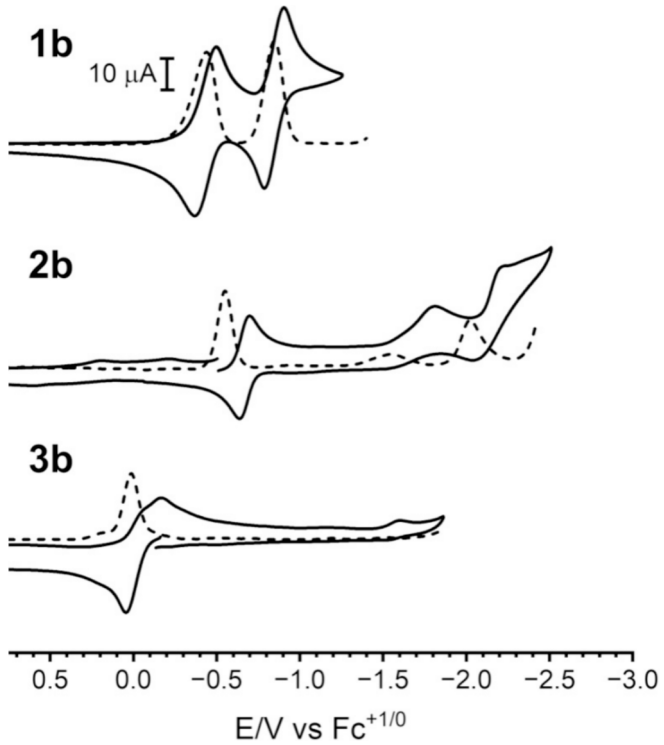

Fig. 6. Cathodic scans of **1b** (top), **2b** (middle), and **3b** (bottom) in 1 mM CH_2Cl_2 (**1b** and **3b**) and THF (**2b**) solutions with 0.1 M *n*-Bu_4NPF_6 as the supporting electrolyte at a 0.1 V/s scan rate.

Table 4
Electrode potentials of observed redox couples (V, vs Fc^{+}/Fc).

	$E_{pa}(Fe^{+4/+3})$	$E_{1/2}$ $(Fe^{+3/+2})$	$E_{pc}(TEIM^{0/-1})$
1b	–	−0.43	−0.84
2b	1.2[a]	−0.66	−2.3[a]
3b	1.5[a]	0.05	–

[a]Irreversible.

methyl substituents. An irreversible $Fe^{+4/+3}$ oxidation of **1b** is also present in the anodic scan (Fig. S2). A reversible $Fe^{+3/+2}$ couple occurs in **2b** at −0.66 V, which is shifted from that of **1b** by approximately −230 mV, reflecting the donor capacity of the azido ligand as noted earlier for the cobalt analogues **1a** and **2a**. Additionally, an ECE (electrochemical-chemical-electrochemical) event is seen for **2b** following the Fe reduction, which is likely caused by the dissociation of an N_3^- upon the reduction of the macrocycle. An irreversible oxidation appears for **2b** in the anodic scan (Fig. S3). In contrast, the ferrous complex **3b** features a readily accessible oxidation ($Fe^{+3/+2}$) at 0.05 V. The return wave of this oxidation is much broader than that of a reversible couple, which is plausibly related to the non-innocent behavior of the NO_2^- ligands.

3.6. Electron paramagnetic resonance

Continuous-wave (CW) X-band EPR was performed at 8 K using 2 mM solutions of **1b** and **2b** in a 1:1 mixture of acetonitrile and toluene to elucidate the electronic structure and ground state of the ferric complexes (Fig. 7). The spectra obtained were simulated using EasySpin, and the corresponding data along with the fitting parameters are listed in Table 5. EPR simulation of complexes **1b** and **2b** reveal that both are axial, low-spin S = ½ Fe^{III} species. However, complex **1b** exhibits a slightly more rhombic signal. In line with Griffith's theory, originally developed for low-spin ferric porphyrin complexes, a ground state configuration of $(d_{xy})^2(d_{xz},d_{yz})^3$ is typically indicated by a large maximum g-value ($g_{max} \approx 3$) and a total g-square sum (Σg^2) of 16. Conversely, a $(d_{xz},d_{yz})^4(d_{xy})^1$ ground state is generally associated with an axial EPR spectrum, a g_{max} less than 2.6, and a Σg^2 less than 16 [23–26]. For compounds **1b** and **2b**, the g_{max} values were found to be less than 2.6, and the observed Σg^2 values for **1b** and **2b** are 14.77 and 13.61, respectively. These findings suggest that **1b** and **2b** possess a $(d_{xz}, d_{yz})^4(d_{xy})^1$ ground state configuration. This conclusion aligns with the short Fe-N bond distances noted in their crystal structures. The α-diimine ligands on the TIM macrocycle act as effective π acceptors, leading to a stabilization of the dπ-orbitals in the Fe(III) center and, consequently, lower energies for the d_{xz} and d_{yz} orbitals.

4. Conclusions

A series of Co^{III} and $Fe^{III/II}$ complexes supported by a new tetra-imine macrocycle, TEIM, has been investigated. Although the solubility of new M(TEIM) complexes has not been improved from that of the M(TIM) analogues, the ease of ligand modification opens the door for future studies to further extend the alkyl substituents or to introduce more elaborate functional groups on the methyl substituents. Modification of macrocycles has been shown to significantly alter the photochemical and electrochemical properties of the metal center in structurally similar cobalt complexes [27]. These continuing efforts aim to generate organometallic complexes supported by tetra-imine macrocycles with the potential to mediate radical-induced organic transformations [28].

CRediT authorship contribution statement

Jeremy J. Roos: Investigation. **Prakhar Gautam:** Writing – original draft, Investigation. **Maximilian P. Martin:** Investigation. **Leobardo Rodriguez Segura:** Writing – original draft, Investigation. **Andrew T. Poore:** Investigation, Data curation. **Shiliang Tian:** Writing – original draft, Data curation. **Aanuoluwapo E. Adeniyi:** Data curation. **Justin L. Andrews:** Data curation, Formal analysis. **Tong Ren:** Writing – review & editing, Writing – original draft, Conceptualization.

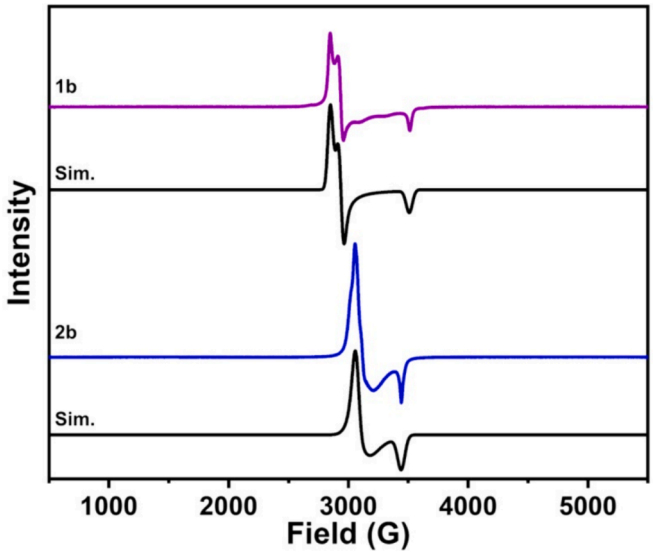

Fig. 7. CW X-band EPR spectra of **1b** (purple) and **2b** (blue) in 1:1 acetonitrile/toluene solution. EasySpin simulations are presented below their respective spectra (black). Conditions: temperature 8 K, modulation amplitude 2 G, microwave power 10.0 mW, and microwave frequency ~ 9.50 GHz.

Table 5
EPR Parameters and spin analysis.

Compound	g values	Σg^2
1b	2.38 2.311.93	14.77
2b	2.21 2.181.97	13.61

Declaration of competing interest

The authors declare that they have no known competing financial interests or personal relationships that could have appeared to influence the work reported in this paper.

Data availability

All data is included in the attached Supplementary data.

Acknowledgements

This work is supported by the U.S. National Science Foundation (CHE 2102049) and by the donors of ACS Petroleum Research Fund under Grant PRF 66514-ND3.

Appendix A. Supplementary data

Supplementary data to this article can be found online at https://doi.org/10.1016/j.poly.2024.117101.

References

[1] S.C. Jackels, D.H. Busch, E.K. Barefield, N.J. Rose, K. Farmery, Some tetragonal cobalt(III) complexes containing tetradentate macrocyclic amine ligands with different degrees of unsaturation, Inorg. Chem. 11 (1972) 2893.

[2] A.M. Tait, D.H. Busch, 2,3,9,10-TETRAMETHYL-1,4,8,11-TETRAAZACYCLOTETRADECA-1,3,8,1O-TETRAENE (2,3,9,10-Me4 [141 -1,3,8,10-tetraene-l,4,8,1 I-N,) COMPLEXES, Inorg. Syn. 18 (1978) 22.
[3] X.L. Hu, B.S. Brunschwig, J.C. Peters, Electrocatalytic hydrogen evolution at low overpotentials by cobalt macrocyclic glyoxime and tetraimine complexes, J. Am. Chem. Soc. 129 (2007) 8988.
[4] C.R. Hess, T. Weyhermuller, E. Bill, K. Wieghardt, [{Fe(tim)}$_2$]: An Fe-Fe dimer containing an unsupported metal-metal bond and redox-active N_4 macrocyclic ligands, Angew. Chem. Int. Ed. 48 (2009) 3703.
[5] C.R. Hess, T. Weyhermuller, E. Bill, K. Wieghardt, Influence of the redox active ligand on the reactivity and electronic structure of a series of Fe(TIM) complexes, Inorg. Chem. 49 (2010) 5686.
[6] L. Rodriguez Segura, R.A. Clendening, T. Ren, Further exploration of Aza-cobalt-cyclobutenes on CoIII(TIM) complexes: Reactivity and spectroelectrochemistry, Organometallics 42 (2023) 1717.
[7] L. Rodriguez Segura, T. Ren, Formation of an Aza-cobalt-cyclobutene on CoIII (TIM): hidden noninnocence of the TIM ligand, Organometallics 41 (2022) 1130.
[8] J. Malme, R.A. Clendening, R. Ash, T. Curry, T. Ren, J. Vura-Weis, Nanosecond metal-to-ligand charge transfer state in an Fe(II) chromophore: Lifetime enhancement via nested potentials, J. Am. Chem. Soc. 145 (2023) 6029.
[9] D.W. Reichgott, N.J. Rose, Photoassisted oxidation of methanol catalyzed by a macrocyclic iron complex, J. Am. Chem. Soc. 99 (1977) 1813.
[10] *APEX4 v2022.10-1, Saint V8.40B,* (2022) Bruker AXS, Inc.
[11] *SHELXTL suite of programs, version 6.14,* (2000-2003) Bruker AXS Inc.
[12] *SHELXL2019,* (2019).
[13] G.M. Sheldrick, SHELXT–Integrated space-group and crystal-structure determination, Acta Cryst. (2015).
[14] G.M. Sheldrick, Crystal structure refinement with SHELXL, Acta Crystallogr. C 71 (2015) 3.
[15] D.S. Eggleston, S.C. Jackels, Tetrasubstituted [14]-1,3,8,10-tetraeneN4 macrocyclic complexes: Synthesis, organic precursor, and template reaction mechanism, Inorg. Chem. 19 (1980) 1593.
[16] D.A. Baldwin, R.M. Pfeiffer, D.W. Reichgot, N.J. Rose, Synthesis and reversible ligation studies of new low-spin iron(II) complexes containing a planar cyclic tetradentate ligand and other donor molecules including carbon-monoxide, J. Am. Chem. Soc. 95 (1973) 5152.
[17] J. Ouyang, B. Na, G. Xiong, L. Xu, T. Jin, Determination of solubility and thermodynamic properties of benzophenone in different pure solvents, J. Chem. Eng. Data 63 (2018) 1833.
[18] L. Rodriguez Segura, S.A. Lee, B.L. Mash, A.J. Schuman, T. Ren, A series of mono- and bis-alkynyl Co(III) Complexes supported by a tetra-imine macrocyclic ligand (TIM), Organometallics 40 (2021) 3313.
[19] H.W. Baird, S.C. Jackels, A. Lachgar, Structural confirmation of a template reaction mechanism: Structure of dichloro (2,9-dimethyl-3,10-diphenyl-1,4,8,11-tetraazacyclotetradeca-1,3,8,10-tetraene)cobalt(III) hexafluorophosphate, J. Cryst. Spectrosc. 23 (1993) 485.
[20] P. Kitiphaisalnont, S. Thohinung, P. Hanmungtum, N. Chaichit, S. Patrarakorn, S. Siripaisarnpipat, Effect of metal ions and length of alkylene bridge on the strength of hydrogen bonds in diiminedioxime cobalt(III) and nickel(II) complexes, Polyhedron 25 (2006) 2710.
[21] R.D. Shannon, C.T. Prewitt, Effective ionic radii in oxides and fluorides, Acta Cryst. B25 (1969) 925.
[22] P. Gautam, R.A. Clendening, A.T. Poore, S. Tian, T. Ren, Fe(III) Bis-Alkynyls supported by the TIM macrocycle: Molecular and electronic structures and altering the nature of charge transfer transitions through reduction, Organometallics 43 (2024) 695.
[23] J.S. Griffith, Theory of electron resonance in ferrihaemoglobin azide, Nature 180 (1957) 30.
[24] J.S. Griffith, Theory of Epr in low-spin ferric haemoproteins, Mol. Phys. 21 (1971) 135.
[25] F.A. Walker, H. Nasri, I. Turowska-Tyrk, K. Mohanrao, C.T. Watson, N. V. Shokhirev, P.G. Debrunner, W.R. Scheidt, pi-acid ligands in Iron(III) porphyrinates. Characterization of low-spin Bis(tert-butylisocyanide) (porphyrinato)iron(III) complexes having (dxz, dyz)4(dxy)1 ground states, J. Am. Chem. Soc. 118 (1996) 12109.
[26] M.K. Safo, G.P. Gupta, C.T. Watson, U. Simonis, F.A. Walker, W.R. Scheidt, Models of the cytochromes b. Low-spin bis-ligated (porphinato) iron (III) complexes with unusual molecular structures and NMR, EPR, and Mössbauer spectra, J. Am. Chem. Soc. 114 (1992) 7066.
[27] K. Shichijo, Y. Kametani, Y. Shiota, K. Yoshizawa, M. Fujitsuka, H. Shimakoshi, Effect of macrocycles on the photochemical and electrochemical properties of cobalt-dehydrocorrin complex: Formation and investigation of Co(I) species, Inorg. Chem. 62 (2023) 11758.
[28] S.H. Kyne, G. Lefèvre, C. Olliver, M. Petit, V.-A. Ramis Cladera, L. Fensterbank, Iron and cobalt catalysis: New perspectives in synthetic radical chemistry, Chem. Soc. Rev. 49 (2020) 8501.